Supplementary Materials

Photoluminescent Carbon-Nitrogen Quantum Dots as Efficient Electrocatalyst for Oxygen Reduction

Jianhua Shen[a], Yunfeng Li[b], Yunhe Su[a], Yihua Zhu[a], Hongliang Jiang[a], Xiaoling Yang[a], Chunzhong Li[a]*

[a] Key Laboratory for Ultrafine Materials of Ministry of Education, School of Materials Science and Engineering, East China University of Science and Technology, Shanghai 200237, China

[b] Shanghai Nanotechnology Promotion Center, Shanghai 200237, China

Email: czli@ecust.edu.cn (C. Li)

*Corresponding author: Fax: +86-21-64250624

Chemicals and materials characterization

Chemical. Melamine, glutaraldehyde, Nafion® 117 solution and silver nitrate were purchased from Sigema-Aldrich. And all other chemicals were purchased from Shanghai Chemical Reagent Co. All chemicals were used without further purification, and their solutions were prepared in distilled water.

Synthesis of Ag NPs. The Ag NPs with an average size of ~40 nm were synthesized using the method introduced by our earlier research[S1]. In a typical synthesis, 0.5 g of $AgNO_3$ and 2.5 g of PVP (MW = 40000) were dissolved in 200 mL of ethylene glycol. This mixture was then heated to 130 ^oC in 20 minute under vigorous stirring. Then, the reaction was allowed to proceed at 130 ^oC for 1 h without further stirring. The Ag NPs were easily separated from the ethylene glycol by addition of 800 mL of acetone, followed by sonication and centrifugation. The precipitates were redispersed in 10 mL of ethanol to obtain the 0.02 g mL^{-1} of Ag NPs/ethanol solution.

Koutecky–Levich plots. The exact kinetic parameters, including electron transfer number (n) and kinetic current density (J_k) involved in the typical ORR process were analyzed based on the Koutecky–Levich (K–L) equation[S2,S3]:

$$\frac{1}{J}=\frac{1}{J_L}+\frac{1}{J_k}=\frac{1}{B\omega^{1/2}}+\frac{1}{J_k} \quad (1)$$

$$B=0.2nFC_o(D_o)^{2/3}\nu^{-1/6} \quad (2)$$

In the Koutecky–Levich equation, J, J_L, J_k are the measured current density, the

diffusion current density, and the kinetic current density, respectively; ω is the rotation speed in rpm, F is the Faraday constant (96485 C mol^{-1}), D_o is the diffusion coefficient of oxygen in 0.1 M KOH (1.9×10^{-5} cm^2 s^{-1}), n is the kinetic viscosity (0.01 cm^2 s^{-1}), and C_o is the bulk concentration of oxygen (1.2×10^{-6} mol cm^{-3}). The constant 0.2 is adopted when the rotation speed is expressed in rpm.

Characterization. Electrochemical experiments were conducted on a CHI 660C electrochemical workstation (CH Instrument Co., China). A conventional three-electrode system included a glassy carbon rotating disk electrode (RDE) (5 mm in diameter, Pine Research Instrumentation) coated with catalysts, a Pt wire counter electrode and an Ag/AgCl (KCl, 3.5 M) reference electrode. Transmission electron microscopy (TEM) studies were performed using a JEM-2100 high-resolution transmission electron microscope equipped with an energy dispersive X-ray analyzer (EDX). The samples were placed on a carbon-coated copper grid and dried at room temperature overnight. X-ray diffraction (XRD) patterns were collected using a powder X-ray diffractometer (RIGAK, D/MAX 2550 VB/PC, Japan). Scanning electron microscopy (SEM) images were recorded on the S-4800 field emission scanning electron microscope at high vacuum with an accelerating voltage of 10 kV. Fourier transform infrared (FTIR) spectra were performed with the transmission module of a Thermo Nicolet 5700 FTIR spectrometer. Thermogravimetric analysis (TGA) of samples was performed using an SDT-Q600 simultaneous TGA/DSC thermogravimetric analyzer (TA Instruments), and the sample was heated under N_2 from room temperature to 800 ^oC at 10 ^oC min^{-1}. X-ray photoelectron spectroscopy

(XPS) was conducted using a VG ESCA 2000 with Mg Kα as the source and using the C 1s peak at 284.6 eV as an internal standard. Photoluminescence spectra were measured on a Fluorolog-3-P UV-VIS-NIR fluorescence spectrophotometer (Jobin Yvon, France). UV-vis spectrum of the CNQDs dispersed in water was obtained using a Unico UV-2102PC spectrophotometer. All spectra were recorded with quartz cells of 10 mm path length.

Quantum Yield (QY) Measurements

Quinine sulfate in 0.5 M sulfuric acid (literature[S4] quantum yield 0.55) was chosen as a standard. The quantum yield of CNQDs in water was calculated according to:

$$\phi = \phi_r \times \frac{A_r}{I_r} \times \frac{I}{A} \times \frac{n^2}{n_r^2} \quad (3)$$

Where Φ is the quantum yield, I is the measured integrated emission intensity, n is the refractive index (1.33 for water), and A is the optical density. The subscript "r" refers to the reference fluorophore of known quantum yield. In order to minimize re-absorption effects, absorbencies in the 10 mm fluorescence cuvette were kept under 0.1 at the excitation wavelength of 365 nm.

Table S1 quantum yield of the as-prepared CNQDs

Sample	Integrated emission intensity (I)	Abs. at 360 nm (A)	Refractive index of solvent (n)	Quantum Yield (Φ)
Quinine sulfate	2295695139	0.0584	1.33	0.55
CNQDs	959374715.6	0.0433	1.33	0.31

References

[S1]. X. Zhang, Y. Zhu, X. Yang, S. Wang, J. Shen, B. Lin, C. Li, Nanoscale 5 (2013) 3359-3366.

[S2]. Y. Liang, Y. Li, H. Wang, J. Zhou, J. Wang, T. Regier, H. Dai, Nature Materials 10 (2011) 780-786.

[S3]. Y. Su, H. Jiang, Y. Zhu, X. Yang, J. Shen, W. Zou, J. Chen, C. Li, Journal of Materials Chemistry A 2 (2014) 7281-7287.

[S4]. H. Xiong, Z. Wang, Y. Xia, Advanced Materials 18 (2006) 748-751.

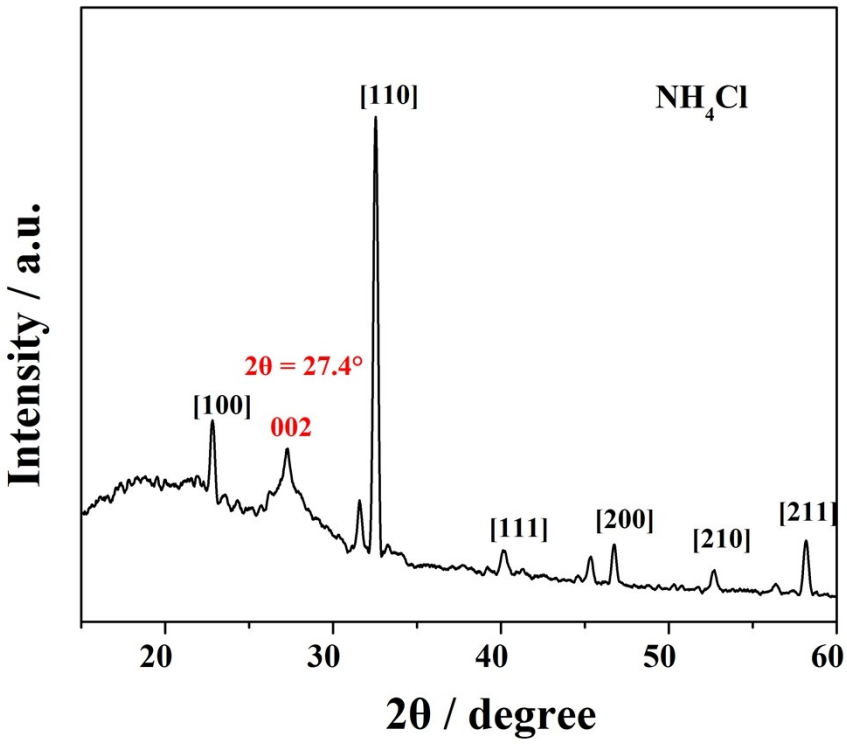

Fig. S1 XRD pattern of the prepared CNQDs without any treatment.

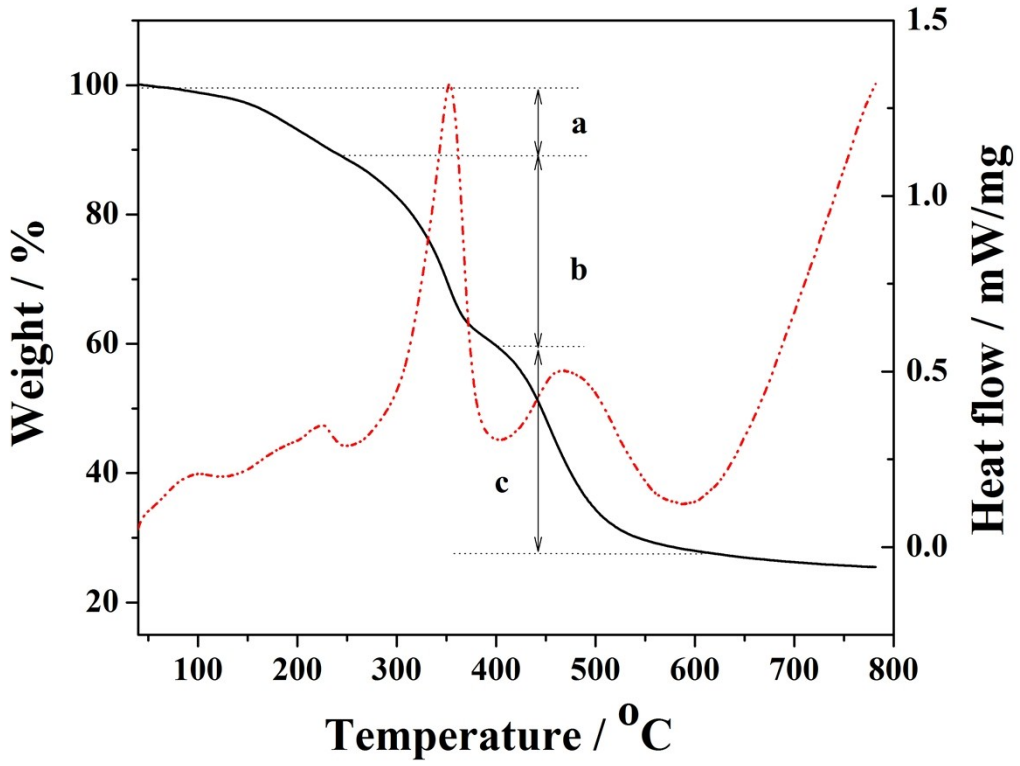

Fig. S2 TGA/DSC thermogravimetric analysis of the products without any treatment.

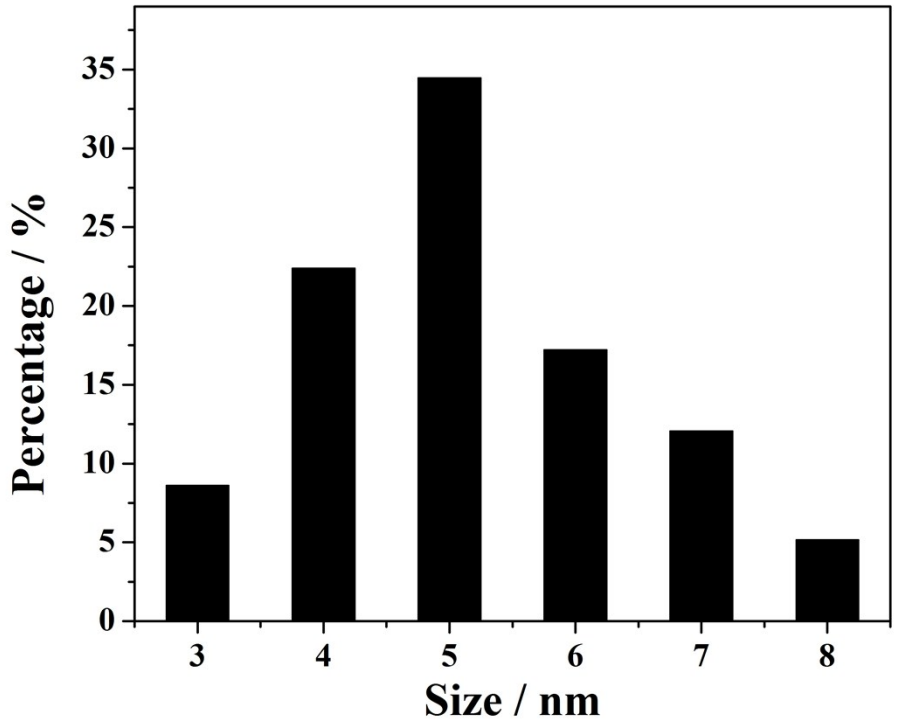

Fig. S3 Diameter distribution of the CNQDs.

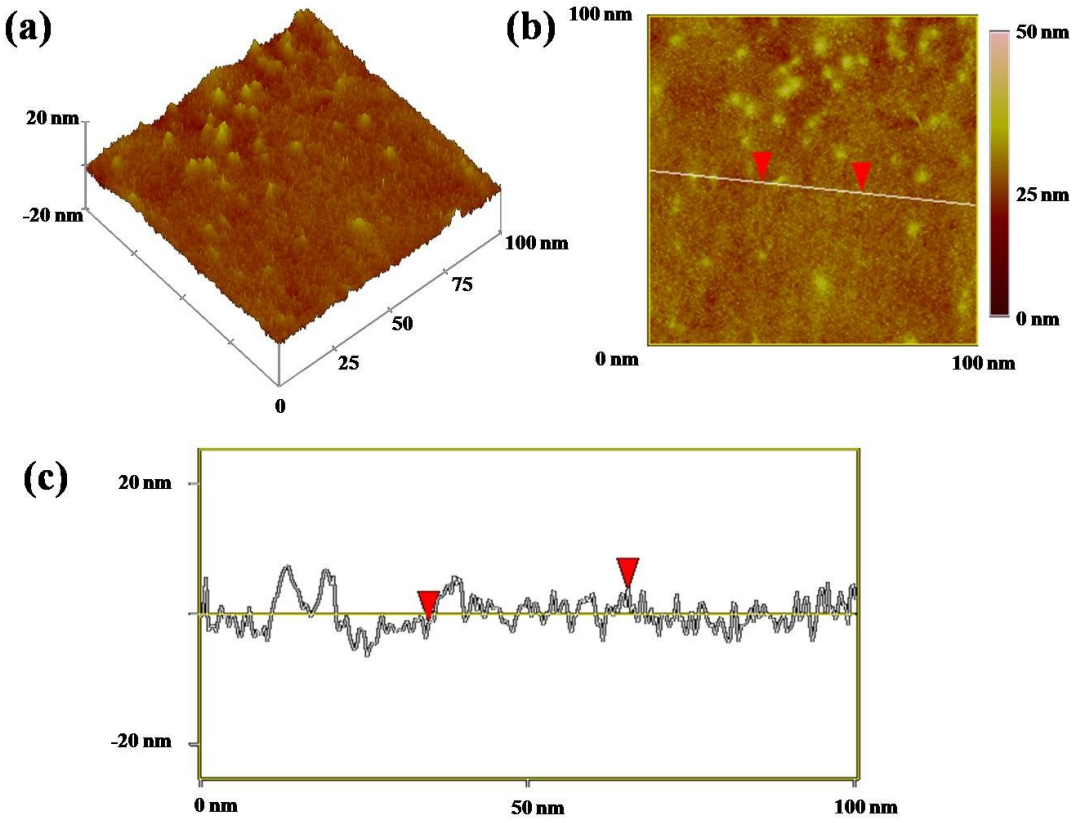

Fig. S4 AFM topography images of the CNQDs on mica substrates.

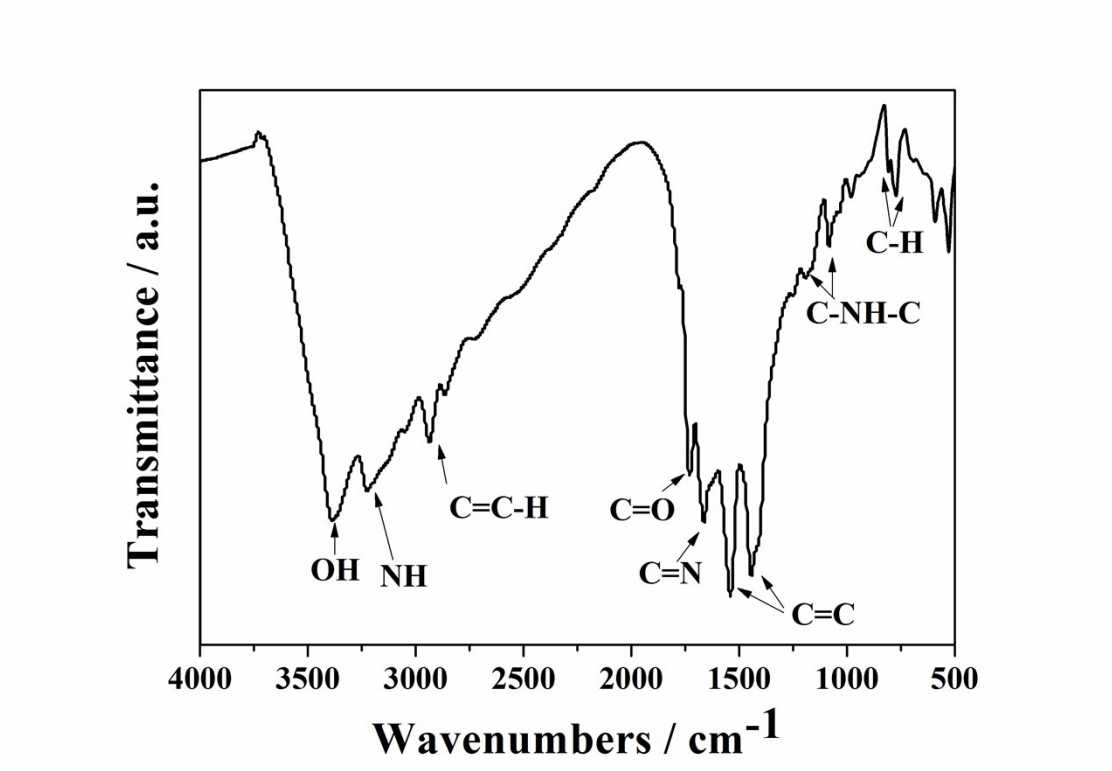

Fig. S5 FTIR spectrum of CNQDs.

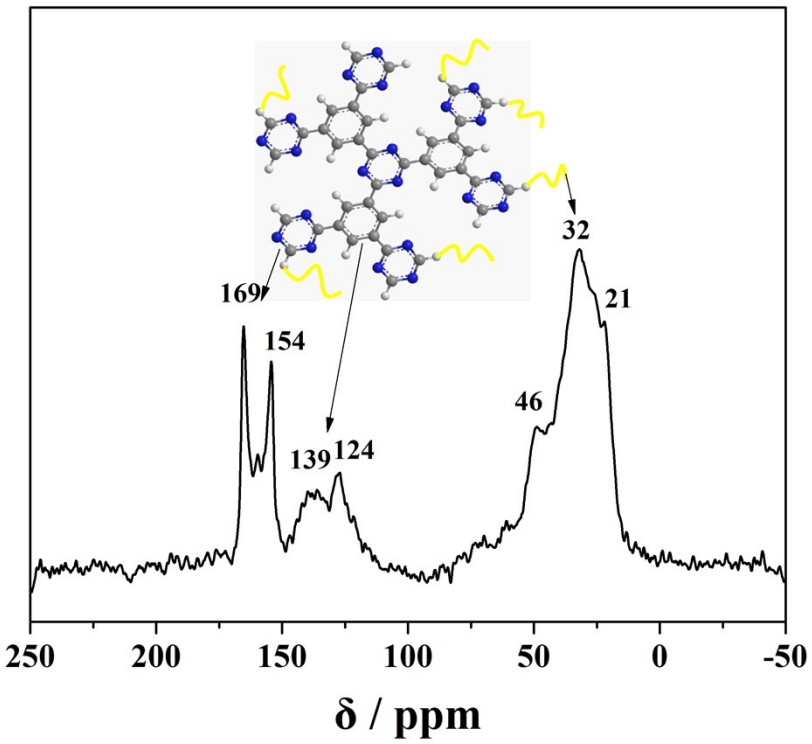

Fig. S6 The solid-state ^{13}C NMR spectrum of CNQDs.

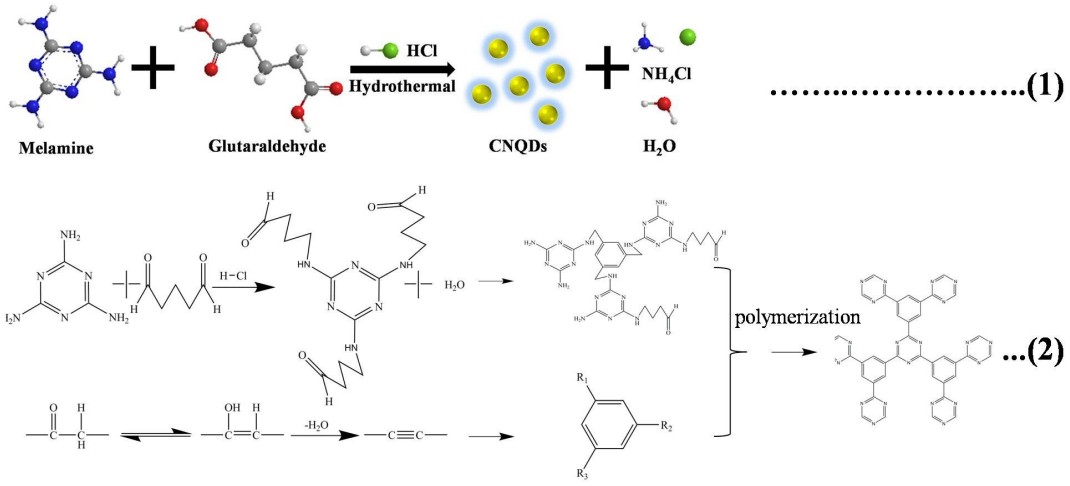

Fig. S7 Schematic illustration of the possible chemical reactions of CNQDs by the hydrothermal treatment.

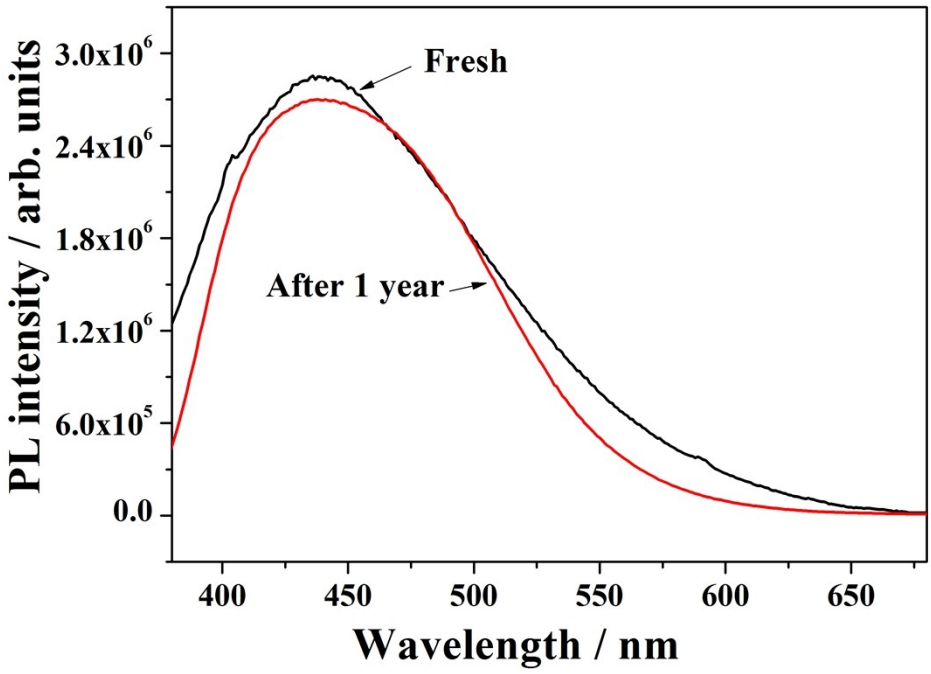

Fig. S8 PL spectra of the CNQDs under 365 nm excitation.

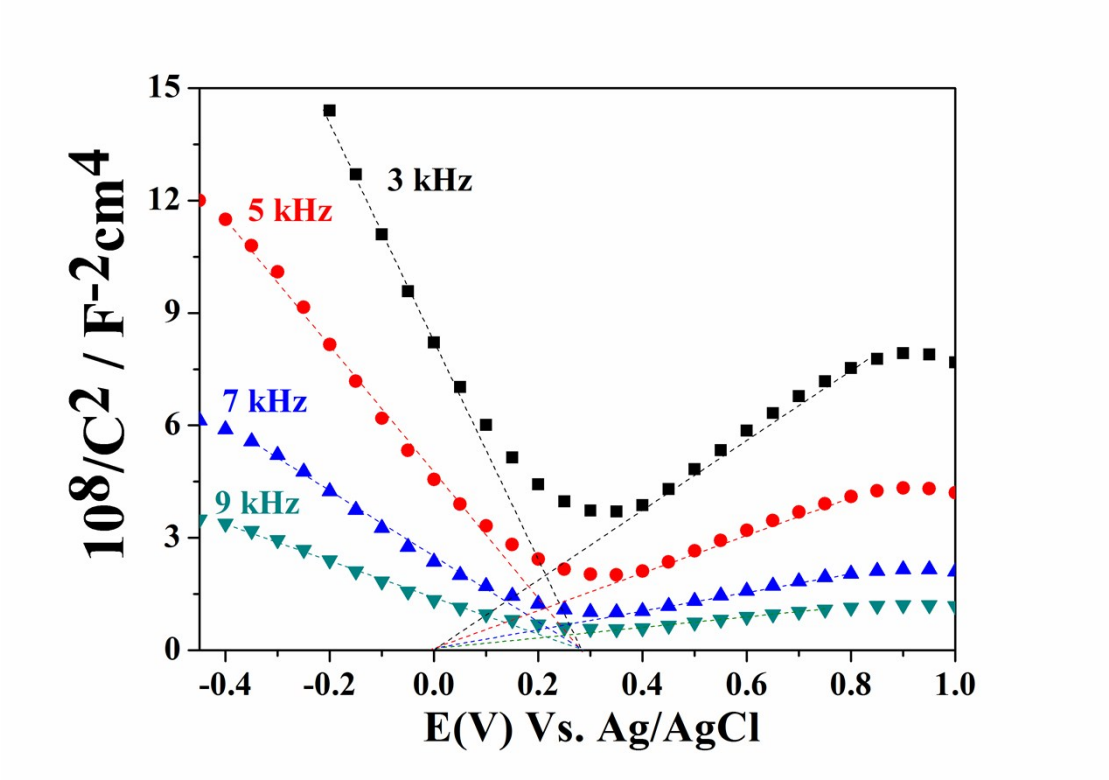

Fig. S9 Variation of capacitance (*C*) with the applied potential in 2 M H_2SO_4 presented in the Mott-Schottky relationship for CNQDs electrode at different frequency. The capacitance was determined by electrochemical impedance spectroscopy.

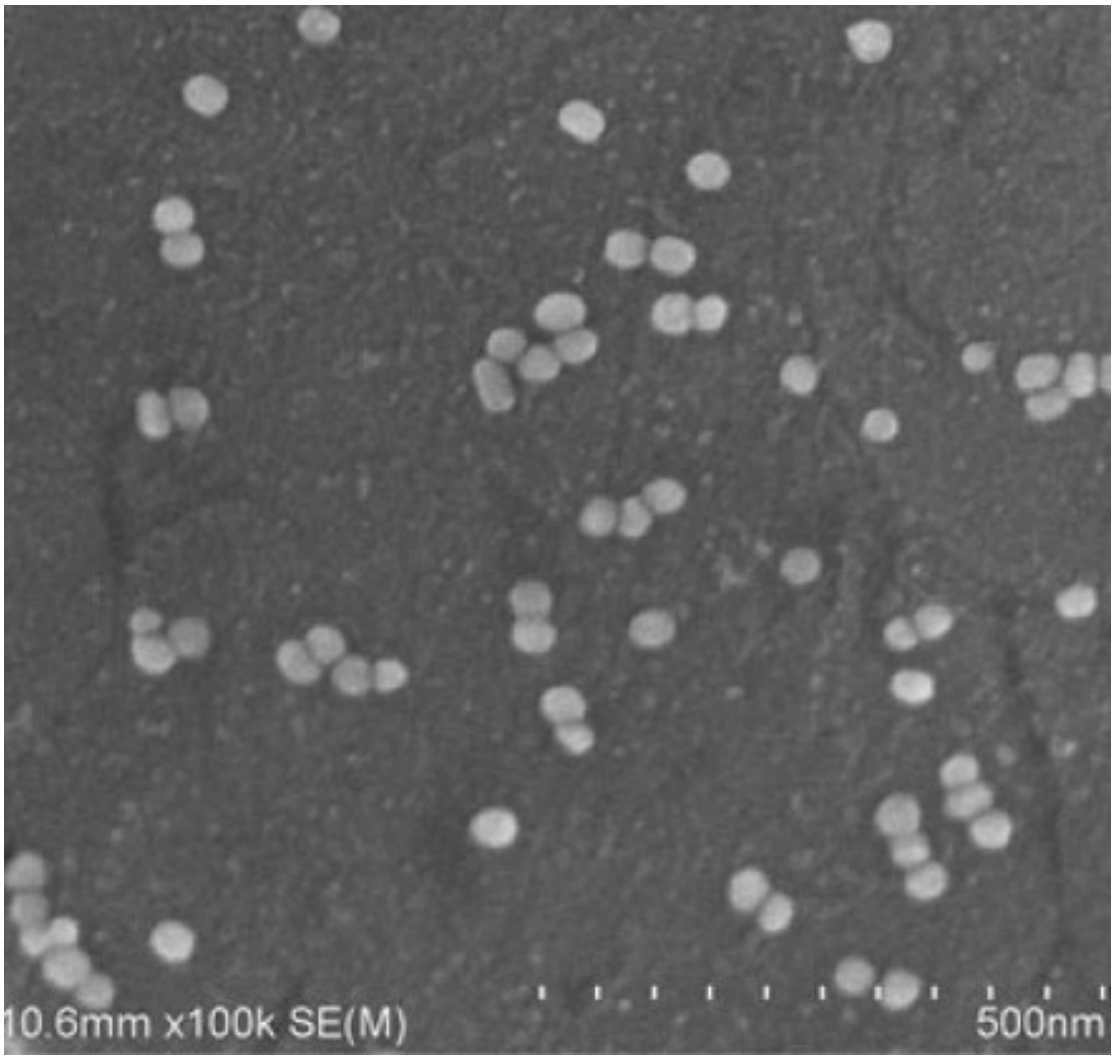

Fig. S10 SEM image of Ag NPs with an average size of ~40 nm.

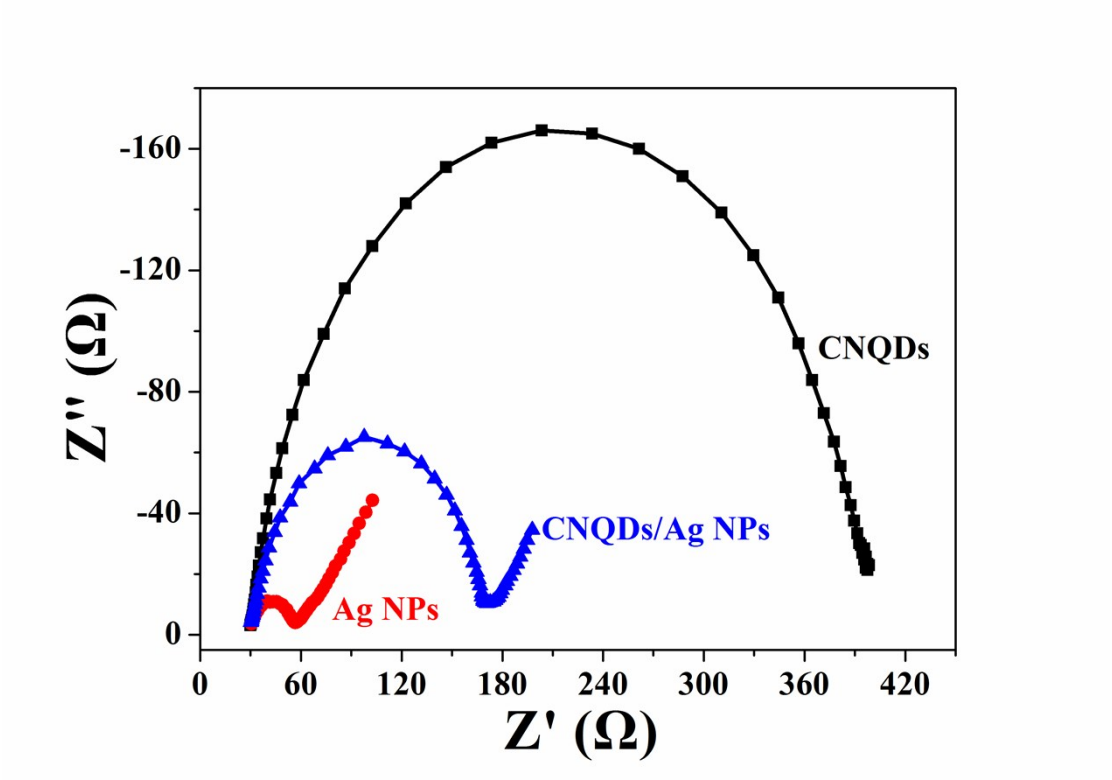

Fig. S11 Impedance spectra of Ag NPs, CNQDs and CNQDs/Ag NPs. The data were recorded in the presence of 1 mM $Fe(CN)6^{3-/4-}$ at E = 0.2V (vs. SCE) with an ac potential modulation amplitude of 10 mV and for frequencies ranging between 100 mHz and 10 kHz.

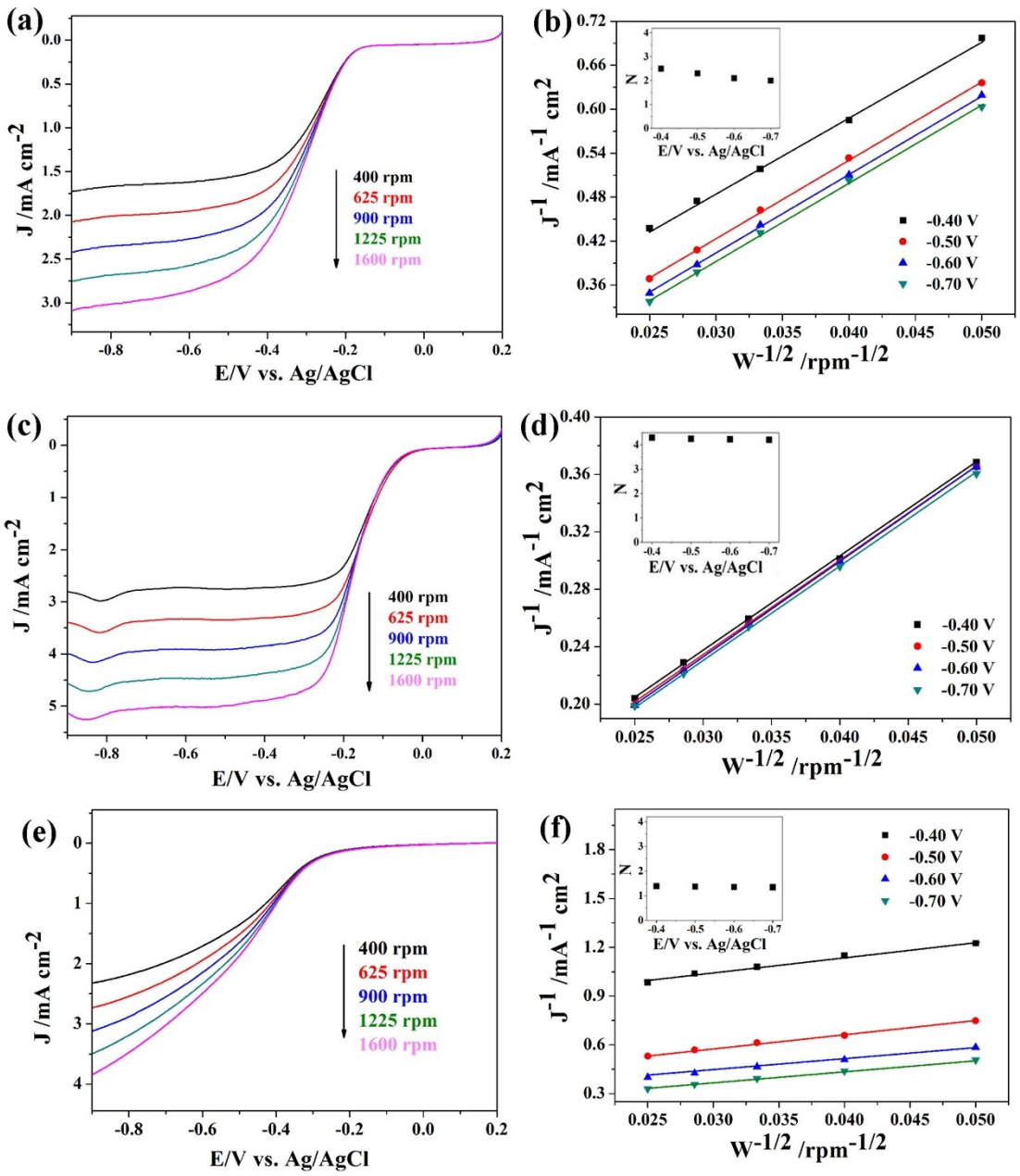

Fig. S12 (a) LSVs for CNQDs in different rotation rate. (b) K-L plots of CNQDs, the inset is the electron transfer number. (c) LSVs for Pt/C in different rotation rate. (d) K-L plots of Pt/C, the inset is the electron transfer number. (e) LSVs for Ag NPs in different rotation rate. (f) K-L plots of Ag NPs, the inset is the electron transfer number.

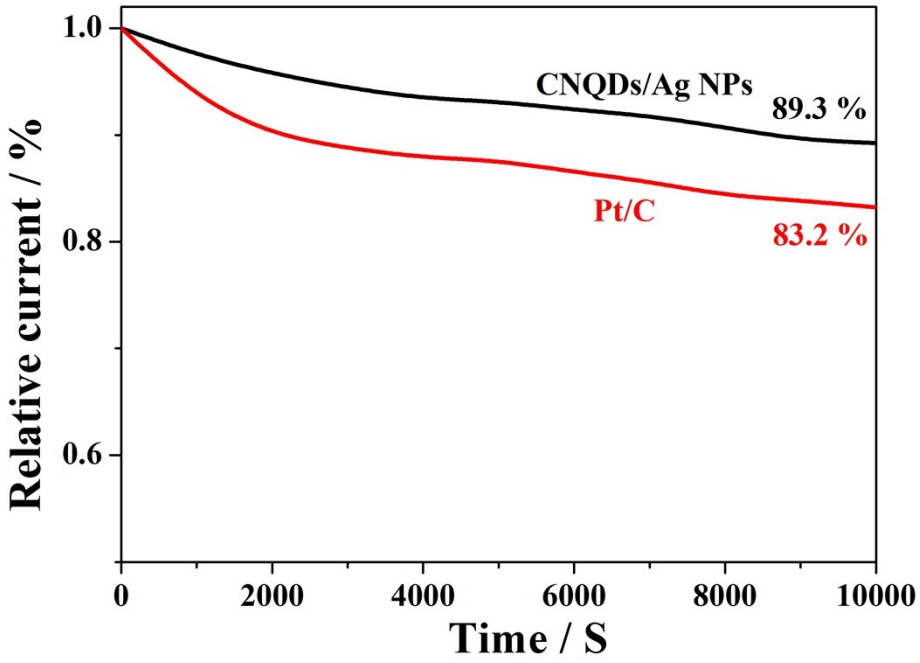

Fig. S13 Chronoamperometry response of CNQDs/Ag NPs and Pt/C in O_2-saturated 0.1 M KOH at -0.4 V with a rotation rate of 900 rpm.